MOLECULAR AND CELLULAR BIOLOGY, Jan. 2008, p. 743–751 Vol. 28, No. 2
0270-7306/08/$08.00+0 doi:10.1128/MCB.01665-07

Disruption of the *Fbxw8* Gene Results in Pre- and Postnatal Growth Retardation in Mice▽†

Takeya Tsutsumi,[1,2] Hiroshi Kuwabara,[1,2] Takehiro Arai,[1,2]
Yonghong Xiao,[3] and James A. DeCaprio[1,2,3]*

Department of Medical Oncology, Dana-Farber Cancer Institute,[1] Department of Medicine, Brigham and Women's Hospital,[2] and Center for Applied Cancer Science, Dana-Farber Cancer Institute,[3] Boston, Massachusetts

Received 8 September 2007/Returned for modification 22 October 2007/Accepted 30 October 2007

CUL7 binds to SKP1, RBX1, and FBXW8 to form a cullin-RING ligase, or an SKP1-cullin-F box protein complex. The targeted disruption of the *Cul7* gene in mice results in significant reduction in embryo size and neonatal lethality. In humans, CUL7 was found to be mutated in the 3-M dwarfism syndrome characterized by severe pre- and postnatal growth retardation, indicating that CUL7 is closely associated with human and mouse growth. We generated mice lacking *Fbxw8* by gene trapping. Similar to *Cul7*$^{-/-}$ animals, *Fbxw8*$^{-/-}$ embryos and placentas were smaller than wild-type and heterozygous littermates and placentas. Approximately 30% of the expected number of *Fbxw8*$^{-/-}$ mice survived birth, but these mice remained smaller than their wild-type and heterozygous littermates throughout postnatal development. FBXW8 expression was detected in most organs of wild-type mice examined, and the organs in Fbxw8$^{-/-}$ mice were smaller than those in wild-type mice. *Fbxw8* expression levels were highest in skeletal muscle, cartilage, and lung tissue. Expression profiling revealed elevated levels of insulin-like growth factor binding protein 1 (IGFBP1) transcripts in *Fbxw8*$^{-/-}$ embryos. Furthermore, we observed increased levels of IGFBP2 in *Cul7*$^{-/-}$ as well as *Fbxw8*$^{-/-}$ fibroblasts. These results demonstrate that the FBXW8-CUL7 complex plays a significant role in growth control.

The ubiquitin-proteasome pathway of protein degradation plays an important role in many biological processes, including cell cycle progression, transcription, and signal transduction. A cascade of three enzymes is involved in the ubiquitin transfer process: the E1 ubiquitin-activating enzyme, the E2 ubiquitin-conjugating enzyme, and the E3 ubiquitin ligase (10). The E3 ubiquitin ligase determines substrate specificity, with subsequent ubiquitination regulated by the E3 activity or the E3-substrate interaction (8). The E3 SKP1-cullin-F box protein (SCF) complex is a well-characterized cullin-RING ligase (CRL) in which CUL1 serves as a scaffold that binds to RBX1, which in turn recruits E2, SKP1, and the F box-containing protein that defines the substrate specificity (13). Sixty-eight human and 74 mouse genes encoding F box-containing proteins have been identified (14).

CUL7 was isolated as a simian virus 40 large T antigen-associated protein and is a member of the CRL family that forms a complex with RBX1, SKP1, and the F box protein FBXW8 (previously referred to as Fbx29 and Fbw6) (1, 2, 9, 15). FBXW8 contains an N-terminal F box motif required for SKP1 binding and a C-terminal WD40 repeat that, by analogy to other FBXW proteins, is predicted to mediate interactions with substrate proteins. CUL7 has not been reported to interact with any other F box protein besides FBXW8, unlike CUL1, which interacts with many F box proteins, including β-transducin repeat-containing protein, FBXW7, and SKP2 (22). CUL7 has also been shown to bind to PARC and GLMN (also known as glomulin and FAP68), although the significance of these interactions is less well understood (2, 25, 26).

Although the substrates of the CUL7-FBXW8 complex are not known, the *Cul7* knockout revealed a significant role in growth and development (2). The targeted disruption of the *Cul7* gene in mice resulted in abnormalities in placental development, embryonic growth retardation, and neonatal lethality due to respiratory failure (2). In addition, *Cul7*$^{-/-}$ mouse embryonic fibroblasts (MEFs) demonstrated a severe proliferation defect compared to MEFs from wild-type or *Cul7*$^{+/-}$ littermates. Recently, the human *CUL7* gene was found to be mutated in individuals with 3-M syndrome, or gloomy-face dwarfism syndrome, characterized by severe pre- and postnatal growth retardation (12, 18). These results indicate an important role for CUL7 in the growth of mice and humans.

Given the effects of *Cul7* mutation on growth, we asked if the disruption of the *Fbxw8* gene, encoding the CUL7-associated F box protein, results in a phenotype similar to that of the *Cul7* knockout. *Fbxw8* null embryos showed severe intrauterine growth retardation, and the majority of the *Fbxw8*$^{-/-}$ mice died neonatally due to respiratory failure. Some *Fbxw8*$^{-/-}$ mice survived birth but remained runted during postnatal development compared to their wild-type and heterozygote littermates. We also observed that the expression of CUL7 was dependent on FBXW8 in a wide variety of tissues. In addition, gene expression profiling revealed the up-regulation of insulin-like growth factor binding protein 1 (IGFBP1) transcripts in *Fbxw8*$^{-/-}$ embryos. In addition, IGFBP2 expression was increased in both *Cul7*$^{-/-}$ and *Fbxw8*$^{-/-}$ MEFs. These results indicate that the CUL7-FBXW8 SCF complex regulates pre- and postnatal growth and development.

* Corresponding author. Mailing address: Dana-Farber Cancer Institute, 44 Binney St., Boston, MA 02115. Phone: (617) 632-3825. Fax: (617) 582-8601. E-mail: james_decaprio@dfci.harvard.edu.

† Supplemental material for this article may be found at http://mcb.asm.org/.

▽ Published ahead of print on 12 November 2007.

MATERIALS AND METHODS

Generation of *Fbxw8* gene trap mice. Male chimeric mice generated from the embryonic stem (ES) cell line RRT057 were obtained from BayGenomics (http://www.genetrap.org) (27). The ES cell line RRT057 was generated by using a gene trap protocol with the trapping construct pGTOLxf, containing a splice-acceptor sequence subcloned toward the 5′ end from the β-geo reporter cassette encoding the β-galactosidase (β-Gal)–neomycin resistance fusion protein. The founder chimera was mated with C57BL/6 females. Mice were genotyped by PCR using primers that identified the β-geo insertion and the wild-type *Fbxw8* genomic sequence. Primer sequences for *Fbxw8* genotyping will be provided upon request.

Cell culture. MEFs were established from embryos isolated at embryonic day 14.5 (E14.5) and cultured in Dulbecco's modified Eagle's medium with 10% fetal bovine serum. For growth curves, 10^5 cells were plated in duplicate into 60-mm dishes and cells were counted twice at 24-h intervals by using a hemocytometer. Serial passage growth over a 3-day interval (expressed as the ratio of the number of cells on day 3 [N3] to the number of cells on day 0 [N0], or the N3/N0 ratio) was determined according to the 3T3 protocol (30). Human lymphoblastoid B-cell lines derived from a 3-M syndrome patient (FY0211) and the patient's parents (FY0212 and FY0213) were obtained from the European Collection of Cell Cultures.

Histological analysis. Embryos and placentas from timed matings of *Fbxw8*$^{+/-}$ mice were fixed in Bouin's fixative (Sigma) and embedded in paraffin. For β-Gal staining, frozen sections of embryos and placentas were prepared and stained according to the protocols of the β-Gal stain manufacturer (Chemicon).

Western blotting and immunoprecipitation. MEFs were lysed in NET-N buffer (20 mM Tris-HCl [pH 8.0], 100 mM NaCl, 1 mM EDTA, 0.5% NP-40) containing protease inhibitor cocktail set I (Calbiochem), and lysates were subjected to immunoblot analysis. For immunoprecipitation, cell lysates were incubated with the corresponding antibody and protein A-Sepharose beads (Amersham) for 3 h and then washed vigorously three times with the lysis buffer before boiling in sodium dodecyl sulfate (SDS) sample buffer. For the determination of tyrosine phosphorylation, MEFs were serum starved for 14 h and treated with a 30-ng/ml concentration of recombinant mouse insulin-like growth factor 1 (IGF1; R&D Systems) for 15 min and then lysed in buffer containing 50 mM Tris-HCl [pH 7.5], 150 mM NaCl, 1% Triton X-100, 10 mM NaF, and 5 mM Na_3VO_4. The rabbit anti-FBXW8 and anti-CUL7 antibodies were generated by Bethyl Laboratories (Montgomery, TX). Additional antibodies used were vinculin (hVIN1; Sigma), SKP1 (Neomarkers), IGFBP2 (R&D Systems), IGF1 receptor (IGF1R [C-20; Santa Cruz]), and phosphotyrosine (PY99; Santa Cruz).

siRNA transfection. Short interfering RNA (siRNA) oligonucleotides were obtained from Dharmacon. Sequences of *CUL7*, *FBXW8*, and luciferase gene siRNA oligonucleotides were as follows: *CUL7* A, AAU CAA CUG CCA UGU CUA CAA; *CUL7* B, AAG AUA CUC CAA CUU CUA CAA; *FBXW8* N1, AAG AUG UGC ACA GGU GAG CAA; *FBXW8* N2, AAG ACG UGG AAG GUG AUU GCA; and luciferase gene siRNA, AAC UUA CGC UGA GUA CUU CGA. Cells in a 6-well plate were transfected with 10 μl of 20 μM oligonucleotides by using Oligofectamine (Invitrogen). Cells were harvested 72 h after transfection and used for immunoblotting.

Quantitative PCR. Total RNA was extracted using an RNeasy mini kit (QIAGEN). Three micrograms of RNA was reverse transcribed using the SuperScript III first-strand synthesis system (Invitrogen). Specific cDNA was quantified by using TaqMan gene expression assays, specific primers, probes for mouse *Cul7* and *Fbxw8* and the mouse β-actin gene, and the real-time PCR 7500 system (Applied Biosystems).

Analysis of secreted proteins. Early-passage MEFs were incubated in 100-mm dishes in Opti-MEM (Invitrogen) for 24 h, and supernatants were harvested for trichloroacetic acid precipitation according to the procedure reported recently (19). The precipitate from trichloroacetic acid was subjected to SDS-polyacrylamide gel electrophoresis (PAGE) and stained with Coomassie blue. The band reproducibly differing in abundance was excised and identified using mass spectrometry.

Transcriptome profiling and Affymetrix data analysis. RNAs were extracted from E18.5 whole embryos by using TRIzol (Invitrogen), subjected to homogenization followed by RNA cleanup with a QIAGEN system, labeled, and hybridized to an Affymetrix GeneChip Mouse Genome 430 2.0 array. Expression data were processed using the R-Bioconductor package Affy (www.bioconductor.org). The preferred analysis methods (5) were used to generate expression values for each probe set. The details of the analysis will be provided upon request.

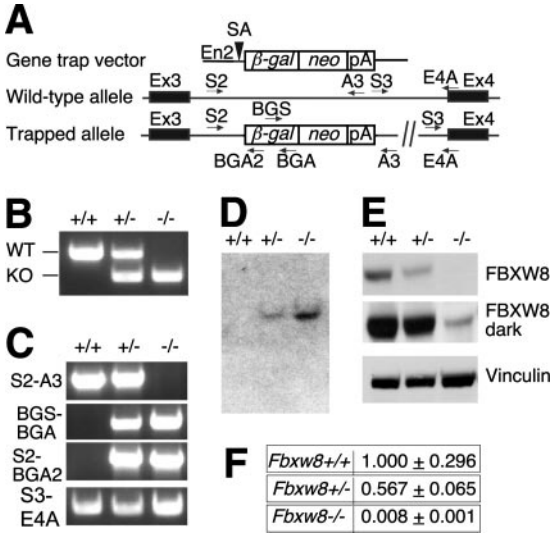

FIG. 1. Characterization of *Fbxw8* gene trap mice. (A, top panel) Schematic representation of the gene trap vector. The gene trap vector contains a splice acceptor (SA) sequence followed by the β-geo fusion containing the *lacZ* and neomycin transferase (*neo*) genes and a polyadenylation sequence (pA). (Middle panel) Partial genomic sequence of the mouse *Fbxw8* gene showing exons 3 and 4 (Ex3 and Ex4; closed rectangles). The PCR primers used for genotype screening are shown (arrows). (Bottom panel) Partial schematic of the *Fbxw8* mutant allele. (B) PCR screening of tail DNA prepared from the offspring of *Fbxw8*$^{+/-}$ intercrosses. The wild-type (WT) and gene-trapped (knockout [KO]) alleles were amplified by the S2-A3 and BGS-BGA primer sets, respectively. (C) PCRs for confirmation of the genotypes. Primers used for each PCR are indicated. (D) Southern blot analysis. Genomic DNA was digested with AflII and probed with the fragment of the β-geo gene. (E) Western blot analysis of whole-cell lysates from MEFs of the indicated genotype. Vinculin served as a loading control. Dark, darker exposure. (F) Real-time PCR analysis of *Fbxw8* mRNA expression in MEFs. The values were standardized to β-actin mRNA expression, and the level of expression in *Fbxw8*$^{+/+}$ MEFs was set at 1.

RESULTS

Generation of *Fbxw8*$^{-/-}$ mice. Mice were generated from ES cells (RRT057) containing an insertion mutation, or gene trap, in the third intron of the *Fbxw8* gene. The gene trap vector generates a spliced fusion transcript comprising *Fbxw8* and the β-geo cassette encoding β-Gal and neomycin resistance. We determined that the trapping construct was inserted 2.6 kb from the 3′ end of exon 3 of *Fbxw8* in the RRT057 cells by sequencing of genomic DNA (Fig. 1A). A PCR assay was established to distinguish the gene-trapped allele from the wild-type allele (Fig. 1B and C). In addition, Southern blotting with a probe against the β-geo cassette confirmed a single integration with the gene trap (Fig. 1D).

To determine if the gene trap reduced FBXW8 protein expression, lysates prepared from MEFs were Western blotted with an antibody against FBXW8. As shown in Fig. 1E, reduced FBXW8 levels in *Fbxw8*$^{+/-}$ MEFs compared to those in wild-type MEFs were detected, and almost no signal was detected in *Fbxw8*$^{-/-}$ MEFs (Fig. 1E, upper panel). In darker exposures, *Fbxw8*$^{-/-}$ MEFs were found to express a slight amount of FBXW8 relative to that in wild-type or heterozygote MEFs (Fig. 1E, middle panel). Real-time PCR revealed that the level of *Fbxw8* mRNA expression in heterozygote MEFs

was 57% and that in homozygous mutant MEFs was 0.8% of the level in wild-type MEFs (Fig. 1F).

Growth retardation of *Fbxw8*$^{-/-}$ mice. Similar to *Cul7*$^{+/-}$ mice, heterozygous *Fbxw8*$^{+/-}$ mice were fertile and indistinguishable in appearance and behavior from their wild-type littermates. An analysis of embryos derived from heterozygote intercrosses revealed that the percentage of *Fbxw8*$^{-/-}$ mice varied between 22 and 24% at E12.5 to E18.5, indicating that *Fbxw8*$^{-/-}$ mice were viable until late in gestation, although some fetal loss cannot be excluded since the numbers of *Fbxw8*$^{-/-}$ as well as *Fbxw8*$^{+/-}$ embryos were smaller than expected relative to the number of *Fbxw8*$^{+/+}$ embryos. Relative to heterozygote littermates, *Fbxw8*$^{-/-}$ embryos were reduced in size (to 83% of littermate size) at E12.5 and became progressively smaller (to 67% of littermate size) by E18.5 but were otherwise normal in appearance. At each gestational stage, *Fbxw8*$^{-/-}$ placentas were also significantly reduced in size. The weight of *Fbxw8*$^{-/-}$ placentas was 60 to 67% that of wild-type placentas, whereas the weights of heterozygous and wild-type placentas were similar to each other (Fig. 2A).

All E18.5 embryos recovered from the uteri of *Fbxw8*$^{+/-}$ intercross mice were alive, as indicated by spontaneous movement and beating hearts. However, all *Fbxw8*$^{-/-}$ E18.5 embryos ($n = 15$) were unable to initiate or sustain strong and regular breathing and quickly turned cyanotic. In contrast, nearly all *Fbxw8*$^{+/+}$ and *Fbxw8*$^{+/-}$ E18.5 embryos began spontaneous breathing. A histological examination of lungs obtained from E18.5 embryos revealed reduced alveolar space in *Fbxw8*$^{-/-}$ lungs (Fig. 3B) compared to that in wild-type lungs (Fig. 3A), indicating a failure to inflate. These results are similar to those observed in *Cul7*$^{-/-}$ mice, which also showed small embryonic and placental sizes, with neonatal lethality resulting from respiratory failure (2). Although neonatal lethality was completely penetrant for *Cul7* null mice, some *Fbxw8* null mice survived birth and lived until weaning. Of 203 offspring from *Fbxw8*$^{+/-}$ intercrosses weaned at 3 weeks of age, only 17 (8%) were *Fbxw8* null, while 58% were heterozygous and 34% were of the wild type (Fig. 2A). This ratio indicated that approximately 70% of *Fbxw8*$^{-/-}$ mice died soon after birth.

We closely examined all surviving mice from several litters over a number of months. As shown in Fig. 2B, both male and female *Fbxw8*$^{-/-}$ mice were smaller than *Fbxw8*$^{+/+}$ or *Fbxw8*$^{+/-}$ mice. *Fbxw8*$^{-/-}$ mice were approximately 70% of the weight of the wild-type and heterozygous mice of the same sex at 1 month of age. Serial examination revealed that although *Fbxw8*$^{-/-}$ mice gained weight, they grew at a lower rate than their heterozygous and wild-type littermates and remained runted in comparison. *Fbxw8*$^{-/-}$ mice appeared normal except for their small size.

Several pairs of *Fbxw8*$^{-/-}$ and *Fbxw8*$^{+/+}$ mice were sacrificed at 3 months of age. FBXW8 protein expression was readily detected in most organs, except for the brains, of wild-type but not *Fbxw8*$^{-/-}$ mice (Fig. 2C). In addition, the organs in *Fbxw8*$^{-/-}$ mice were proportionally smaller, except for the brains, the sizes of which were similar to those of the brains of wild-type mice (Fig. 2D). Detailed histopathological examination, however, revealed no significant abnormalities in *Fbxw8*$^{-/-}$ mice (data not shown). Since bone abnormalities in 3-M patients with mutations of *CUL7* have been observed

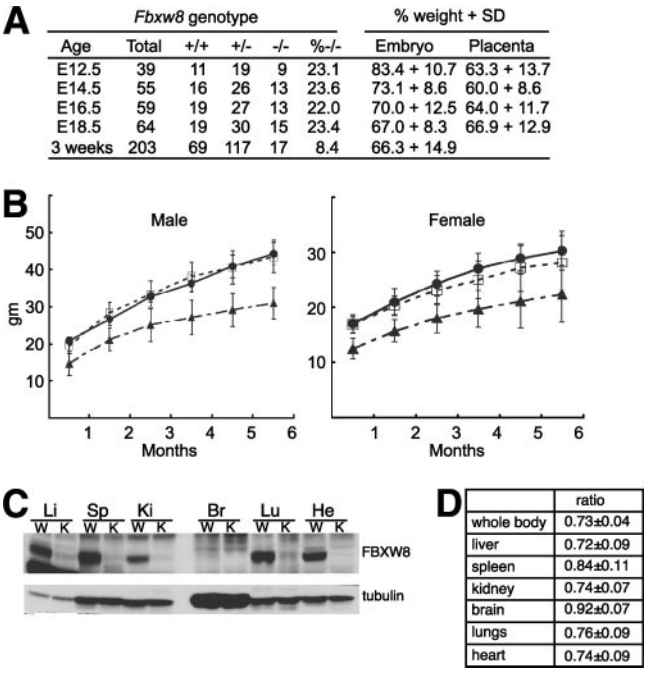

FIG. 2. Neonatal death and growth retardation of *Fbxw8*$^{-/-}$ mice. (A) Genotypes and phenotypes of *Fbxw8*$^{+/-}$ intercrosses. % −/−, proportion of viable *Fbxw8*$^{-/-}$ embryos and pups at each stage; % weight, average weight of *Fbxw8*$^{-/-}$ embryos as a percentage of the average weight of *Fbxw8*$^{+/-}$ littermates (SD, standard deviation). The weights of *Fbxw8*$^{+/+}$ and *Fbxw8*$^{+/-}$ embryos were indistinguishable (data not shown). (B) Growth curves for surviving male (left) and female (right) mice. The average weights of *Fbxw8*$^{+/+}$ (circles; male, 10; female, 6), *Fbxw8*$^{+/-}$ (squares; male, 15; female, 14), and *Fbxw8*$^{-/-}$ (triangles; male, 11; female, 14) mice at each month are shown. (C) FBXW8 expression in adult tissues. Lysates were prepared from organs of 3-month-old *Fbxw8*$^{+/+}$ (wild-type [W]) and *Fbxw8*$^{-/-}$ (knockout [K]) mice and blotted with an anti-FBXW8 antibody. Li, liver; Sp, spleen; Ki, kidney; Br, brain; Lu, lung; He, heart. (D) Weights of organs in mice. Five pairs of *Fbxw8*$^{-/-}$ and *Fbxw8*$^{+/+}$ mice were sacrificed, and the weights of organs were examined. The weights of the bodies or organs of *Fbxw8*$^{-/-}$ mice were divided by those of *Fbxw8*$^{+/+}$ mice, and the results are shown as ratios ± standard deviations.

frequently, we examined the vertebral bodies (lumbar vertebra 5) and femurs of *Fbxw8*$^{-/-}$ mice. Micro-computed tomography scanning of the vertebral bodies and femurs revealed no specific abnormalities in the overall shape (data not shown).

FBXW8 expression in embryos and placentas. The gene trap vector enabled the determination of the tissue-specific expression pattern of *Fbxw8*, since the β-geo fusion protein derived from the insertion was under the control of the endogenous *Fbxw8* promoter. We assayed for β-Gal expression in histologic sections of *Fbxw8*$^{-/-}$ embryos and placentas. In E18.5 embryos, β-Gal was highly expressed in skeletal muscle, with intense staining observed in the diaphragms, intercostals, and abdominal walls (Fig. 3C). Muscles in the extremities were also stained. Smooth muscle cells had slight, if any, β-Gal expression. In addition, β-Gal staining in developing bone was observed (Fig. 3E). Under higher magnification, we observed that β-Gal was expressed in the epiphyses of tubular bones, corresponding to cartilage, but not in the diaphyses, where the formation of bone in E18.5 embryos had already occurred (Fig.

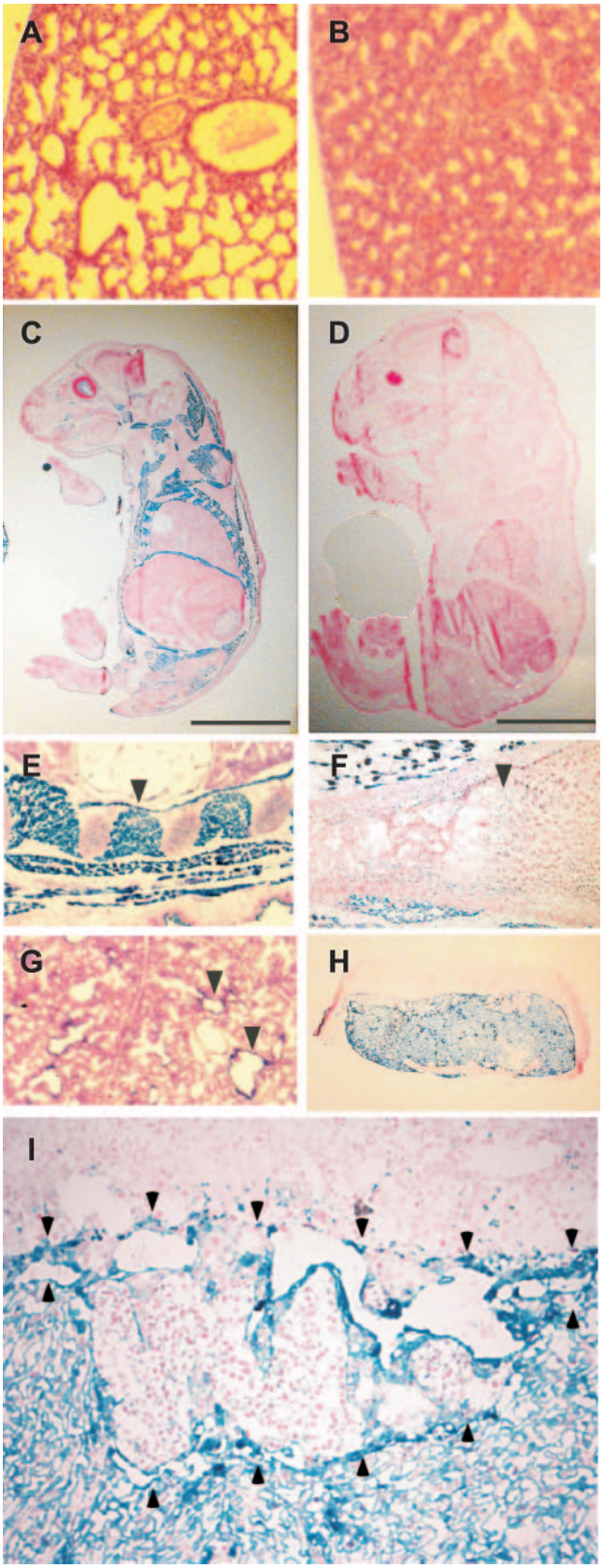

3F). We also detected β-Gal expression in the lungs, specifically in the bronchial epithelia (Fig. 3G). Weak β-Gal expression was detected in kidneys, eyes, and skin, and little, if any, was detected in the brains. Heterozygote E18.5 embryos showed a similar pattern of expression, although at reduced levels compared to those in the homozygote mutant embryos (data not shown). In addition, E14.5 mutant embryos showed a pattern of expression similar to that in E18.5 mutant embryos, with no significant differences (data not shown).

When *Fbxw8*$^{-/-}$ mutant placentas were examined, intense β-Gal staining was detected in the labyrinthine layer (Fig. 3H). Moderate expression was also detected in the spongiotrophoblast layer, but not in the decidual layer. We observed a thin and relatively disorganized spongiotrophoblast layer in *Fbxw8*$^{-/-}$ placentas compared to that in the wild-type and heterozygote placentas, similar to the spongiotrophoblast layer in *Cul7*$^{-/-}$ placentas (Fig. 3I) (2, 32).

FBXW8 protein expression and CUL7 protein expression are mutually dependent. We have previously detected the specific interaction of CUL7 with FBXW8 by using epitope tag constructs and have reported that the expression of FBXW8 protein was reduced in *Cul7*$^{-/-}$ cells compared to that in wild-type MEFs (2, 9). To determine if the endogenous CUL7, FBXW8, and SKP1 proteins interact, immunoprecipitations from MEFs as well as cells from human cell lines were performed with monospecific antibodies against CUL7 and FBXW8 and immunoprecipitates were analyzed by Western blotting. Immunoprecipitation analysis of CUL7 and FBXW8 in mouse and human cells revealed the coprecipitation of these proteins as well as SKP1 (Fig. 4A).

We have reported that in *Cul7*$^{-/-}$ MEFs, FBXW8 protein expression was reduced due to a significantly shorter half-life than that in wild-type MEFs (2). To determine if CUL7 expression was affected by the disruption of the *Fbxw8* gene, lysates were prepared from wild-type and *Fbxw8* null MEFs, as well as from whole E18.5 embryos and placentas. As shown in Fig. 4B, the expression of CUL7 was decreased in *Fbxw8*$^{-/-}$ cells and tissues relative to that in wild-type cells and tissues, and conversely, FBXW8 was reduced in *Cul7*$^{-/-}$ cells and tissues. To determine if CUL7 protein expression in *Fbxw8*$^{-/-}$ MEFs was decreased due to a shorter half-life, protein synthesis was inhibited with cycloheximide. In wild-type MEFs, the level of CUL7 was stable, with no detectable decrease in signal after 8 h of cycloheximide treatment (Fig. 4C). In contrast, CUL7 levels in *Fbxw8*$^{-/-}$ MEFs began to decrease after 2 h of cycloheximide treatment and were nearly undetectable at 8 h.

FIG. 3. Histology and FBXW8 expression in embryos and placentas. (A and B) The lungs of E18.5 *Fbxw8*$^{-/-}$ embryos were unable to inflate (B), in contrast to those of *Fbxw8*$^{+/+}$ littermates (A). (C and D) β-Gal staining of sagittally sectioned E18.5 embryos followed by counterstaining with nuclear fast red. β-Gal activity was strongly detected in the skeletal muscles of an *Fbxw8*$^{-/-}$ embryo (C) but not in those of an *Fbxw8*$^{+/+}$ embryo (D) (bars, 5 mm). (E and F) β-Gal expression (indicated by arrowheads) was detected in bone (E), especially in the epiphysis (arrowhead) of tubular bone corresponding to cartilage (F). (G) β-Gal was highly expressed in the bronchiolar epithelium (arrowheads). (H and I) β-Gal staining of the placenta was detected in the labyrinthine and spongiotrophoblast layers (arrowheads).

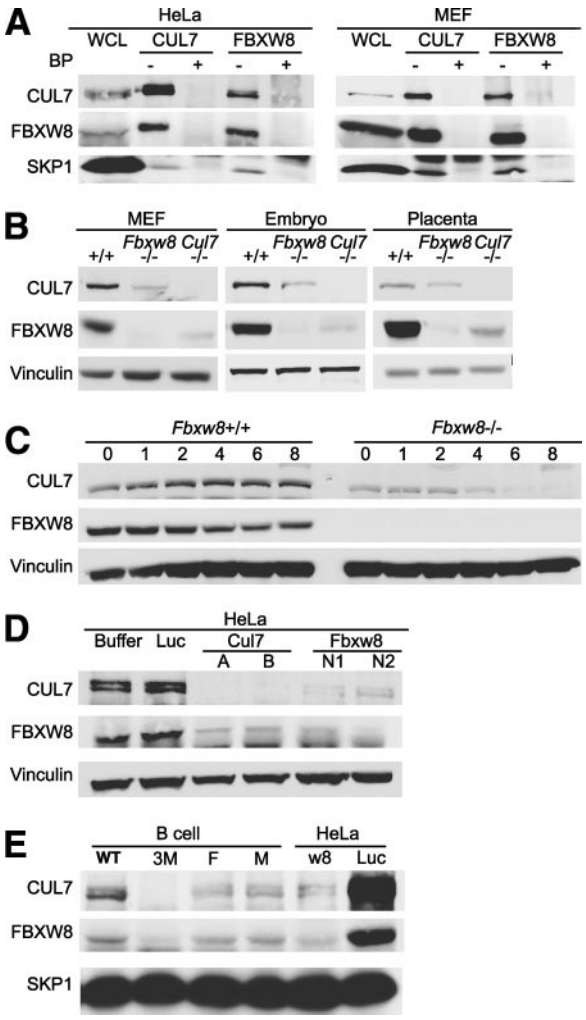

FIG. 4. CUL7 and FBXW8 expression. (A) Interaction of CUL7, FBXW8, and SKP1 in human and mouse cells. Lysates from HeLa cells and MEFs were immunoprecipitated with anti-CUL7 (BL1541) or anti-FBXW8 antibody and analyzed by immunoblotting with anti-CUL7 (BL653), anti-FBXW8, and anti-SKP1 antibodies. Blocking peptide (BP) was added to lysates before immunoprecipitation to confirm the specific interaction with the immunoprecipitating antibody. WCL, whole-cell lysate; −, absent; +, present. (B) FBXW8 and CUL7 expression in *Fbxw8*$^{-/-}$ and *Cul7*$^{-/-}$ tissues. Cell lysates prepared from wild type (+/+) or mutant (−/−) MEFs, embryos, and placentas were analyzed by immunoblotting with anti-CUL7, anti-FBXW8, and antivinculin (loading-control) antibodies. (C) CUL7 stability in *Fbxw8*$^{-/-}$ MEFs. MEFs were treated with 50 ng of cycloheximide/ml and harvested at the time points indicated above the lanes (numbers are hours of cycloheximide treatment). (D) HeLa cells were transfected with two different siRNA oligonucleotides targeting *CUL7* (A and B) and *FBXW8* (N1 and N2) and an siRNA oligonucleotide targeting the luciferase gene (Luc) as a control. (E) Whole-cell lysates were prepared from a lymphoblastoid B-cell line derived from a 3-M syndrome individual (3M) and compared to cells from the father (F), the mother (M), and an individual expressing wild-type CUL7 (WT) and HeLa cells transfected with siRNA oligonucleotides targeting *FBXW8* (w8) or the luciferase gene (Luc).

We examined the expression of *Cul7* mRNA by reverse transcription-quantitative PCR and found similar expression levels in wild-type and *Fbxw8*$^{-/-}$ MEFs (data not shown), indicating that the decrease in protein stability accounted for the decreased CUL7 expression in *Fbxw8*$^{-/-}$ MEFs. Similar results were confirmed with *Cul7*$^{-/-}$ MEFs and tissues, where we observed decreased FBXW8 expression due to a decrease in protein stability (Fig. 4b).

To determine if CUL7 and FBXW8 expression levels were mutually dependent in human cells, we transfected HeLa cells with siRNA against *CUL7* or *FBXW8*. Using two different siRNAs specific for each gene, we observed decreased expression of FBXW8 when CUL7 levels were reduced and reduced levels of CUL7 when FBXW8 was knocked down relative to levels in mock- or control-transfected siRNA-treated cells (Fig. 4D).

Individuals with 3-M syndrome were previously reported to have mutations in both alleles of *CUL7* (12). We determined that the FY211 lymphoblastoid B-cell line derived from an individual with 3-M syndrome contains the mutation 263delT, causing a valine-to-alanine substitution followed by a short nonsense sequence (V88A plus 25 residues) resulting in a truncated protein (see Fig. S1 in the supplemental material). We examined the cell line from the 3-M syndrome patient as well as the heterozygote lines from the patient's parents for CUL7 and FBXW8 protein expression. Full-length CUL7 protein was not detected in lysates prepared from the 3-M cells but could readily be detected in the parental cells (Fig. 4E). Notably, the levels of FBXW8 expression in the 3-M syndrome patient cells were also decreased compared to those in the parental cell lines (Fig. 4E). These results strongly support the model in which CUL7 protein expression and FBXW8 protein expression are dependent on each other.

Increased IGFBP1 expression in *Fbxw8*$^{-/-}$ embryos. To explore the phenotype of *Fbxw8*$^{-/-}$ embryos, transcriptome profiling of E18.5 *Fbxw8*$^{-/-}$ and *Fbxw8*$^{+/-}$ whole embryos was carried out. We selected *Fbxw8*$^{+/-}$ embryos as controls since they also contained the β-geo integrated gene trap that might affect the expression of some genes. Five *Fbxw8*$^{-/-}$ and five *Fbxw8*$^{+/-}$ embryos were profiled from an initial batch of three each and a second batch of two each to increase detection power. Though both batches had a large number of genes differentially expressed, when all 10 expression profiles were analyzed together, only *Fbxw8*, the trapped gene, showed significant differential expression. When results from the two batches of *Fbxw8*$^{-/-}$ and *Fbxw8*$^{+/-}$ embryos were compared, only nine genes consistently showed differential expression in the same direction, with a *q* value (false discovery rate if the *P* value is significant) cutoff of 0.2 (Table 1). In addition to *Fbxw8*, most of the down-regulated genes were muscle related. The only gene up-regulated in *Fbxw8*$^{-/-}$ embryos relative to heterozygous embryos was the IGFBP1 gene. Quantitative PCR analysis confirmed the elevated expression of IGFBP1 mRNA in *Fbxw8*$^{-/-}$ embryos compared to that in their heterozygous littermates (data not shown).

Increased IGFBP2 expression in *Cul7*$^{-/-}$ and *Fbxw8*$^{-/-}$ MEFs. We had previously noted that fibroblasts from *Cul7*$^{-/-}$ embryos grew more slowly than MEFs from their heterozygous or wild-type littermates (2). To determine if *Fbxw8*$^{-/-}$ MEFs also grew slowly, we prepared samples of *Fbxw8*$^{+/+}$, *Fbxw8*$^{+/-}$, and *Fbxw8*$^{-/-}$ MEFs from littermate embryos and determined their growth rates. Equal numbers of passage 2 MEFs were seeded into replicate plates, and the MEFs were fed every 2 days and counted. *Fbxw8*$^{-/-}$ MEFs grew more slowly than

TABLE 1. Genes differentially expressed in *Fbxw8*$^{-/-}$ embryos

Gene	First batch[a]			Second batch[b]		
	Avg ratio of expression[c]	*P* value	*q* value	Avg ratio of expression[c]	*P* value	*q* value
Fbxw8	0.3435	1.29E−09	3.84E−05	0.2722	3.29E−08	4.25E−04
Igfbp1	2.2438	1.13E−05	0.0153	2.2559	1.60E−04	0.0414
Atp2a1	0.5650	6.49E−05	0.0344	0.6923	7.48E−04	0.0870
Actn3	0.5641	7.01E−04	0.1030	0.5139	1.16E−04	0.0361
Mypn	0.6328	1.27E−03	0.1299	0.7429	5.05E−03	0.1823
Ryr1	0.6434	1.35E−03	0.1338	0.6748	2.00E−03	0.1344
Sfrs8	0.6034	1.94E−03	0.1543	0.5034	1.35E−04	0.0380
Mybpc2	0.4275	2.58E−03	0.1713	0.6470	6.11E−04	0.0839
Pcgf5	0.6602	2.69E−03	0.1744	0.6164	1.01E−03	0.1035

[a] The first batch of embryos included three *Fbxw8* null (*Fbxw8*$^{-/-}$) embryos and three heterozygous (*Fbxw8*$^{+/-}$) embryos.
[b] The second batch of embryos included two null embryos and two heterozygous embryos.
[c] Ratio of average expression in null embryos to average expression in heterozygous embryos.

Fbxw8$^{+/+}$ and *Fbxw8*$^{+/-}$ MEFs (Fig. 5A). Similar results were obtained with knockout MEFs from two different litters (data not shown). We attempted to generate immortalized versions of *Fbxw8*$^{-/-}$ MEFs by using serial passage in a 3T3 protocol (30). Growth over a 3-day interval (expressed as the N3/N0 ratio) was examined (Fig. 5B). Wild-type MEFs grew relatively well for 10 passages, but *Fbxw8*$^{-/-}$ MEFs underwent a severe growth arrest within five or six passages without evidence of crisis. A similar growth arrest of *Cul7*$^{-/-}$ MEFs after six passages has been observed previously (data not shown). MEFs were generated from embryos derived from mating *Trp53* null mice with *Fbxw8*$^{+/-}$ mice. *Fbxw8*$^{-/-}$ *Trp53*$^{-/-}$ MEFs grew as rapidly as *Fbxw8*$^{+/+}$ *Trp53*$^{-/-}$ MEFs and showed no evidence of growth arrest after serial passage (data not shown). In contrast, the *Fbxw8* null phenotype, including a small embryo, a dysmorphic placenta, a high incidence of neonatal lethality, and a small adult size, was not suppressed by the loss of *Trp53* (data not shown). Therefore, it appears that the poor growth phenotype of *Fbxw8*$^{-/-}$ MEFs was strongly dependent on wild-type p53 but that the significant developmental defects observed in *Fbxw8*$^{-/-}$ mice were not eliminated by the loss of p53.

Given the growth defect observed in both *Cul7*$^{-/-}$ and *Fbxw8*$^{-/-}$ MEFs, we asked if any secreted proteins were differentially expressed in the tissue culture supernatant. *Cul7*$^{-/-}$ and wild-type MEFs were incubated in reduced-serum medium for 24 h, and supernatants were harvested for analysis by SDS-PAGE. Coomassie blue staining revealed a specific band at 32 kDa that showed consistent up-regulation in *Cul7*$^{-/-}$ MEFs compared to the level in wild-type MEFs (Fig. 5C). The analysis of this band by mass spectrometry yielded eight unique peptides specific to mouse IGFBP2. The presence of increased levels of IGFBP2 in the tissue culture supernatant from *Cul7*$^{-/-}$ MEFs compared to those in the supernatant from wild-type MEFs was confirmed using a specific antibody (Fig. 5D). The concentration of IGFBP2 in the tissue culture supernatant was determined by enzyme-linked immunosorbent assay under a wide variety of growth conditions. We observed that supernatant from *Cul7*$^{-/-}$ MEFs consistently contained two- to threefold-higher levels of IGFBP2 than that from *Cul7*$^{+/+}$ MEFs under a variety of growth conditions (data not shown).

To determine if *Fbxw8*$^{-/-}$ MEFs also expressed higher levels of IGFBP2, lysates from wild-type, *Cul7*$^{-/-}$, and *Fbxw8*$^{-/-}$ MEFs were blotted with an IGFBP2 antibody. Increased expression of intracellular IGFBP2 was detected in *Fbxw8*$^{-/-}$ as well as *Cul7*$^{-/-}$ MEFs compared to that in wild-type MEFs from littermate controls (FIG. 5E). Although we consistently detected elevated levels of IGFBP2 in *Fbxw8*$^{-/-}$ and *Cul7*$^{-/-}$ MEFs, we could not detect the expression of IGFBP1 in MEFs, and there were no differences in the levels of expression of IGFBP3, IGFBP4, or IGFBP5 between wild-type and mutant MEFs (data not shown).

Given the elevated levels of IGFBP2 in *Cul7* and *Fbxw8* mutant MEFs, we tested whether IGFBP2 could be targeted for ubiquitination and subsequent proteasomal destruction by the SKP1-CUL7-FBXW8 CRL complex. We did not observe any specific binding of IGFBP2 to CUL7 or FBXW8 (data not shown). In addition, the levels of IGFBP2 did not change in either mutant or wild-type MEFs when cells were treated with proteasome inhibitors (data not shown). Furthermore, when *Fbxw8*$^{-/-}$ and wild-type MEFS were treated with cycloheximide, we observed that the half-lives of IGFBP2 in wild-type and *Fbxw8* null cells were similar (data not shown). Despite the repeated observation that IGFBP2 levels were elevated in *Fbxw8*$^{-/-}$ and *Cul7*$^{-/-}$ MEFs, we were unable to detect any evidence either that IGFBP2 was a direct substrate for ubiquitination and degradation or that its stability was affected by the CUL7-FBXW8 complex.

The IGFBPs serve to modulate the availability of IGFs to activate the IGF1R tyrosine kinase and downstream signal transducers. To determine if the increased levels of IGFBP2 affected IGF1R signaling, MEFs were serum starved before stimulation with IGF1. In the absence of IGF1, the tyrosine phosphorylation of IGF1R was undetectable in wild-type as well as *Cul7*$^{-/-}$ and *Fbxw8*$^{-/-}$ MEFs. After stimulation with IGF1 for 15 min, tyrosine-phosphorylated IGF1R was readily detected in wild-type MEFs but was detected at reduced levels in *Cul7*$^{-/-}$ and *Fbxw8*$^{-/-}$ MEFs (Fig. 5F). The levels of expression of IGF1R in all cells were similar regardless of IGF1 stimulation. The addition of neutralizing antibodies to IGFBP2 to the tissue culture medium failed to affect the growth rate of knockout MEFs. In addition, the RNA interference-mediated knockdown of IGFBP2 did not affect the proliferation index or the cell cycle profile of *Fbxw8*$^{-}$/$^{-}$ MEFs. Although elevated levels of IGFBP2 in *Fbxw8*$^{-/-}$ and *Cul7*$^{-/-}$ MEFs were consistently observed, we

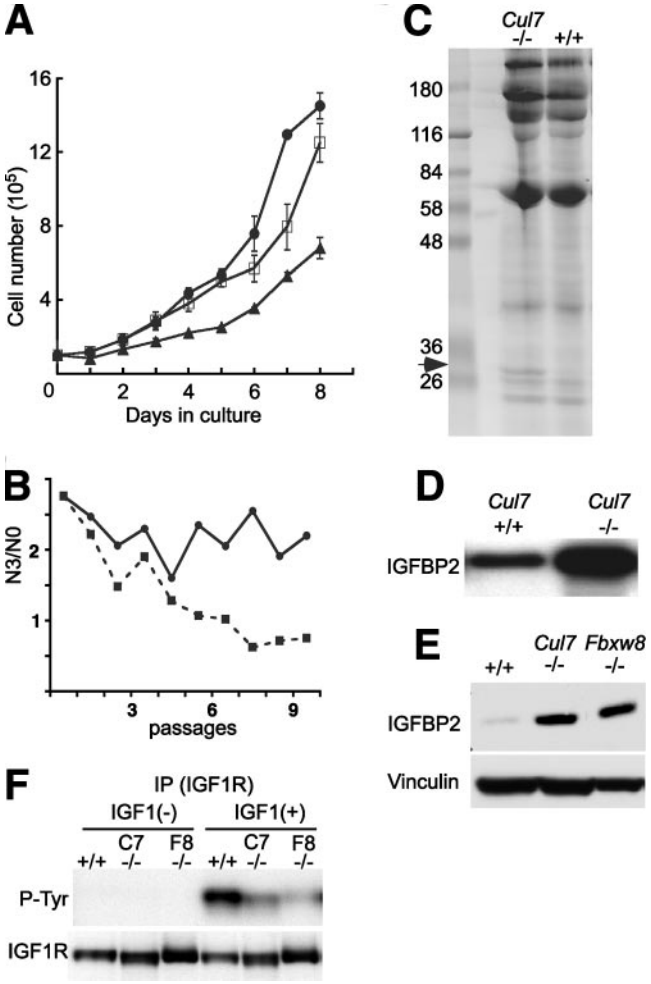

FIG. 5. IGFBP2 up-regulation in *Cul7*$^{-/-}$ and *Fbxw8*$^{-/-}$ MEFs. (A) Passage 2 MEFs (10^5) derived from littermates from *Fbxw8*$^{+/-}$ intercrosses were replica plated into 60-mm dishes and counted in duplicate every 24 h. ●, *Fbxw8*$^{+/+}$; □, *Fbxw8*$^{+/-}$; ▲, *Fbxw8*$^{-/-}$. (B) MEFs from a confluent primary culture were plated into 100-mm dishes at a density of 10^6/dish, grown for 3 days, and counted, and the N3/N0 ratios were determined. The cells were transferred to a new dish at the original cell density, and the N3/N0 ratios were repeatedly calculated. ●, *Fbxw8*$^{+/+}$; □, *Fbxw8*$^{-/-}$. (C) *Cul7*$^{-/-}$ and wild-type MEFs were cultured in Opti-MEM for 24 h, and proteins in the tissue culture supernatant were precipitated with trichloroacetic acid, resolved by SDS-PAGE, and detected by Coomassie blue staining. Mass spectrometry analysis of the band indicated by the arrow revealed IGFBP2. (D) Expression of secreted IGFBP2 in MEFs. Aliquots from the samples in panel C were analyzed by immunoblotting with anti-IGFBP2 antibody. (E) Cell lysates prepared from wild-type (+/+), *Cul7*$^{-/-}$, and *Fbxw8*$^{-/-}$ MEFs were blotted with IGFBP2 and vinculin antibodies. (F) Cell lysates were prepared from MEFs that were serum starved [IGF1(−)] and subsequently treated with IGF1 [IFG1(+)] (C7, *Cul7*$^{-/-}$; F8, *Fbxw8*$^{-/-}$). Lysates were immunoprecipitated (IP) with IGF1R antibody and immunoblotted with phosphotyrosine (P-Tyr) and IGF1R antibodies.

were unable to demonstrate that IGFBP2 contributed to significant growth delay.

DISCUSSION

In this study, we demonstrated that *Fbxw8*$^{-/-}$ mice show a phenotype remarkably similar to that of *Cul7*$^{-/-}$ mice. Key similarities include normal embryonic development except for the significantly decreased sizes of mutant embryos and placentas relative to those of their wild-type and heterozygous littermates and neonatal death due to respiratory failure. A significant difference between the CUL7 and FBXW8 mutant phenotypes was that while all *Cul7*$^{-/-}$ mutant embryos died at birth, approximately 30% of *Fbxw8*$^{-/-}$ mice survived until weaning (2). Mutant *Fbxw8* mice remained runted and grew more slowly than their littermates, although they were otherwise normal in appearance and behavior and did not develop any additional abnormalities. In addition to these developmental similarities, primary *Fbxw8*$^{-/-}$ and *Cul7*$^{-/-}$ MEFs grew more slowly than wild-type and heterozygous cells, indicating that the normal function of CUL7 and FBXW8 contributes to cellular proliferation.

Different methods of gene disruption may account for the survival of some of the *Fbxw8*$^{-/-}$ mice and none of the *Cul7*$^{-/-}$ mice. *Cul7*$^{-/-}$ mice were generated using targeted recombination resulting in the excision of exons 2 to 4 of *Cul7* (2). In contrast, *Fbxw8*$^{-/-}$ mice were generated by the gene trap method. The gene trap eliminated nearly all *Fbxw8* expression, but a small amount of mRNA (<1% of the wild-type level) and protein was detected in the *Fbxw8*$^{-/-}$ MEFs and tissues (Fig. 1E and F and 2C) (16). It is possible that surviving *Fbxw8*$^{-/-}$ mice may express sufficient FBXW8 at a critical stage in development to permit survival.

Alternatively, the phenotype of the *Cul7*$^{-/-}$ mice may be more severe given the possibility that CUL7 may interact with additional F box-containing proteins to yield a more complex phenotype. By analogy, CUL1 is expected to bind many F box proteins, including β-transducin repeat-containing protein 1, SKP2, and FBXW7. The targeted disruption of *Cul1* in mice results in embryonic lethality, whereas the disruption of the F box genes *Btrc* and *Skp2* does not result in lethal phenotypes (20, 21, 34). The *Fbxw7*$^{-/-}$ phenotype is lethal to embryos but is much milder than the *Cul1*$^{-/-}$ phenotype (29, 31). These observations suggest that the severity of the *Cul1* knockout may be due to its effects on multiple F box proteins and their corresponding substrates. Although CUL7 may bind specifically to additional F box proteins, we have failed to observe any specific interaction with an F box-containing protein other than FBXW8. It should be noted that CUL7 but not FBXW8 binds specifically to PARC and GLMN (25, 26). It is possible that the severity of the *Cul7* null phenotype may reflect an adverse impact on these two proteins as well.

It is not clear why the *Cul7* null and *Fbxw8* null embryos had difficulty inflating their lungs at birth. When we examined *Fbxw8* null E18.5 embryos, all failed to inflate their lungs, indicating that this failure was the most significant defect that limited survival. This defect may reflect specific effects in the bronchial epithelial tissues, structural effects related to bone and cartilage development, or other features. It should be noted that a recent report on 3-M syndrome patients revealed a high frequency of respiratory distress at birth frequently necessitating mechanical ventilation (18). It was suggested that abnormal cartilaginous development may have led to respiratory distress in at least one of these 3-M syndrome patients.

We took advantage of the gene trap construct that expressed β-Gal under the control of the endogenous *Fbxw8* promoter to determine the relative levels of FBXW8 expression in embry-

onic tissue. FBXW8 was most highly expressed in skeletal muscle and placental labyrinthine tissues. In addition, FBXW8 was expressed in the growth plates of embryonic bones (Fig. 3). This expression pattern may contribute to the small stature of *Fbxw8*$^{-/-}$ mice, since these tissues are keys factors in determining body size. It is worth noting that many of the genes down-regulated in *Fbxw8*$^{-/-}$ embryos were muscle related, perhaps reflecting high levels of expression of FBXW8 in muscles.

The IGF signaling pathway is an important contributor to fetal and postnatal growth and development. IGF2 is essential for normal mouse embryonic growth (6, 7), whereas IGF1 has a continuous function throughout development (4, 17). A series of mice carrying null mutations of IGF-related genes has been established. The knockout of IGF1, IGF2, IGF1R, or insulin receptor substrate 1 leads to prenatal and postnatal growth retardation, although mice with these mutations have some differences in body size (3, 6, 17, 23, 28). On the other hand, transgenic mice that overexpress IGFBP1 or IGFBP2 show growth retardation (11, 24). Among the null mutants, the *Igf1r*$^{-/-}$ phenotype is similar to the *Cul7*$^{-/-}$ phenotype, with small embryos that die at birth due to respiratory failure (17).

In two independent analyses, we observed that the levels of IGFBP were increased in *Fbxw8* mutant embryos and MEFs. Expression profiling revealed that the only gene significantly overexpressed in whole *Fbxw8*$^{-/-}$ mutant embryos was the IGFBP1 gene. In addition, the purification of secreted proteins from *Cul7*$^{-/-}$ MEFs revealed high levels of IGFBP2, and these increased levels were also observed in *Fbxw8*$^{-/-}$ MEFs. Furthermore, we observed a blunted response to IGF1R signaling in both *Cul7*$^{-/-}$ and *Fbxw8*$^{-/-}$ MEFs. The growth defect in *Fbxw8* mutant embryos and mice may reflect disturbances in IGF signaling due to elevated levels of IGFBPs in the growth plate (33). These results raise the possibility that the loss of *Fbxw8* perturbs the ability of bone and muscle to contribute to the overall growth of the mouse.

Despite the consistent appearance of elevated levels of IGFBP2 in *Fbxw8*$^{-/-}$ MEFs, we were unable to demonstrate that IGFBP2 overexpression contributed to the slow growth of mutant MEFs. Notably, neither blocking antibodies to IGFBP2 that interfered with binding to IGF1 or siRNA that reduced levels of IGFBP increased the growth rate or affected the cell cycle profile of *Fbxw8*$^{-/-}$ MEFs. It is possible that increased IGFBP2 levels and decreased IGF1R activation may not contribute directly to the slow-growth phenotype in *Cul7*$^{-/-}$ or *Fbxw8*$^{-/-}$ MEFs and embryos. Although no studies of human 3-M syndrome patients have reported IGFBP levels, IGFBP isoforms may be elevated and serve as a biomarker of the disease.

While CUL7 and FBXW8 have been detected in nearly all cell lines and tissues tested, differences in the levels of expression have been noted. For example, high levels of CUL7 and FBXW8 were detected in MEFs and HeLa cells while lower levels were observed in lymphoblastoid B-cell lines. Of note, we were unable to detect significant levels of FBXW8 protein expression in adult mouse brains (Fig. 2C). Similarly, as indicated by the β-Gal expression pattern, little FBXW8 was expressed in the embryonic brains (Fig. 3C). In addition, the sizes of the brains from wild-type and *Fbxw8*$^{-/-}$ null mice were more similar to each other than the sizes of any other organs tested (Fig. 2D). These results suggest that the brain may be less influenced by the absence of FBXW8, since there is little expression normally. It should also be noted that the human 3-M short-stature syndrome is characterized by relatively normal head size.

In addition to the reduced size of the *Fbxw8* null mice, we observed a reduced growth rate of *Fbxw8*$^{-/-}$ MEFs compared to that of heterozygote and wild-type MEFs (Fig. 5A). We also observed a severe defect in the ability of the *Fbxw8* knockout MEFs to be serially passaged (Fig. 5B). Similar defects in growth rates and passage number were also observed for *Cul7*$^{-/-}$ MEFs (2). In addition, we have observed that the expression of CUL7 is strongly dependent on levels of FBXW8 and vice versa (Fig. 4). These results support our model that CUL7 and FBXW8 form an SCF-like complex that contributes to growth and proliferation.

During the preparation of this work, Tsunematsu and colleagues reported the phenotype of *Fbxw8*$^{-/-}$ mice generated by a conventional targeted knockout strategy (32). Similar to the results in our study, about one-third of *Fbxw8* null mice in that study were born alive, despite severe defects in placental development. However, there were several differences from our study, including the deaths of approximately two-thirds of the *Fbxw8*$^{-/-}$ embryos between E12.5 and E17.5. In addition, it was reported that the lungs of the *Fbxw8* knockout mutant embryos inflated well. Although we cannot rule out the possibility that some null embryos generated in our study died prior to birth, we have repeatedly observed the respiratory defect in the E18.5 *Fbxw8* null embryos.

Two recent studies revealed that *CUL7* mutations were present in patients with 3-M syndrome, a disorder characterized by intrauterine growth retardation and severe postnatal dwarfism (12, 18). These mutations in *CUL7* reduced the E3 ubiquitin ligase activity of CUL7 and disrupted the interaction of CUL7 with FBXW8 and SKP1. Interestingly, Yakut patients with the 3-M short-stature syndrome have few bone abnormalities but have a high frequency of neonatal respiratory distress and abnormal vascularization of the fetal placenta (18). These phenotypes were very similar to those observed in *Fbxw8*$^{-/-}$ as well as *Cul7*$^{-/-}$ mice. It is noteworthy that the small size and decreased growth rate of the mutant *Fbxw8* mice may predict that individuals with other short-stature syndromes, or with non-*CUL7* related 3-M syndrome, may have mutations in the *FBXW8* gene.

ACKNOWLEDGMENTS

This work was supported in part by Public Health Service grant RO1 CA093804 from the National Cancer Institute. T.T. was supported in part by the Toyobo Biotechnology Foundation.

We thank Roderick Bronson and Gerald Chu at the Dana-Farber/Harvard Cancer Center Rodent Histopathology Core, William Lane at the Harvard Microchemistry and Proteomics Analysis Facility, and Edward Fox at the Dana-Farber Microarray Core Facility. The ES cell line was obtained from the National Heart, Lung, and Blood Institute-funded Program for Genomic Applications at BayGenomics. We thank Elizabeth Bland and Peter Scambler for identifying the CUL7 mutation in the 3-M syndrome patient cell line.

REFERENCES

1. **Ali, S. H., J. S. Kasper, T. Arai, and J. A. DeCaprio.** 2004. Cul7/p185/p193 binding to simian virus 40 large T antigen has a role in cellular transformation. J. Virol. **78:**2749–2757.

2. **Arai, T., J. S. Kasper, J. R. Skaar, S. H. Ali, C. Takahashi, and J. A. DeCaprio.** 2003. Targeted disruption of p185/Cul7 gene results in abnormal vascular morphogenesis. Proc. Natl. Acad. Sci. USA **100:**9855–9860.
3. **Araki, E., M. A. Lipes, M. E. Patti, J. C. Bruning, B. Haag, III, R. S. Johnson, and C. R. Kahn.** 1994. Alternative pathway of insulin signalling in mice with targeted disruption of the IRS-1 gene. Nature **372:**186–190.
4. **Baker, J., J. P. Liu, E. J. Robertson, and A. Efstratiadis.** 1993. Role of insulin-like growth factors in embryonic and postnatal growth. Cell **75:**73–82.
5. **Choe, S. E., M. Boutros, A. M. Michelson, G. M. Church, and M. S. Halfon.** 2005. Preferred analysis methods for Affymetrix GeneChips revealed by a wholly defined control dataset. Genome Biol. **6:**R16.
6. **DeChiara, T. M., A. Efstratiadis, and E. J. Robertson.** 1990. A growth-deficiency phenotype in heterozygous mice carrying an insulin-like growth factor II gene disrupted by targeting. Nature **345:**78–80.
7. **DeChiara, T. M., E. J. Robertson, and A. Efstratiadis.** 1991. Parental imprinting of the mouse insulin-like growth factor II gene. Cell **64:**849–859.
8. **Deshaies, R. J.** 1999. SCF and Cullin/Ring H2-based ubiquitin ligases. Annu. Rev. Cell Dev. Biol. **15:**435–467.
9. **Dias, D. C., G. Dolios, R. Wang, and Z. Q. Pan.** 2002. CUL7: a DOC domain-containing cullin selectively binds Skp1.Fbx29 to form an SCF-like complex. Proc. Natl. Acad. Sci. USA **99:**16601–16606.
10. **Hershko, A., and A. Ciechanover.** 1998. The ubiquitin system. Annu. Rev. Biochem. **67:**425–479.
11. **Hoeflich, A., M. Wu, S. Mohan, J. Foll, R. Wanke, T. Froehlich, G. J. Arnold, H. Lahm, H. J. Kolb, and E. Wolf.** 1999. Overexpression of insulin-like growth factor-binding protein-2 in transgenic mice reduces postnatal body weight gain. Endocrinology **140:**5488–5496.
12. **Huber, C., D. Dias-Santagata, A. Glaser, J. O'Sullivan, R. Brauner, K. Wu, X. Xu, K. Pearce, R. Wang, M. L. Uzielli, N. Dagoneau, W. Chemaitilly, A. Superti-Furga, H. Dos Santos, A. Megarbane, G. Morin, G. Gillessen-Kaesbach, R. Hennekam, I. Van der Burgt, G. C. Black, P. E. Clayton, A. Read, M. Le Merrer, P. J. Scambler, A. Munnich, Z. Q. Pan, R. Winter, and V. Cormier-Daire.** 2005. Identification of mutations in CUL7 in 3-M syndrome. Nat. Genet. **37:**1119–1124.
13. **Jackson, P. K., and A. G. Eldridge.** 2002. The SCF ubiquitin ligase: an extended look. Mol. Cell **9:**923–925.
14. **Jin, J., T. Cardozo, R. C. Lovering, S. J. Elledge, M. Pagano, and J. W. Harper.** 2004. Systematic analysis and nomenclature of mammalian F-box proteins. Genes Dev. **18:**2573–2580.
15. **Kasper, J. S., H. Kuwabara, T. Arai, S. H. Ali, and J. A. DeCaprio.** 2005. Simian virus 40 large T antigen's association with the CUL7 SCF complex contributes to cellular transformation. J. Virol. **79:**11685–11692.
16. **Li, J., X. Zhu, M. Chen, L. Cheng, D. Zhou, M. M. Lu, K. Du, J. A. Epstein, and M. S. Parmacek.** 2005. Myocardin-related transcription factor B is required in cardiac neural crest for smooth muscle differentiation and cardiovascular development. Proc. Natl. Acad. Sci. USA **102:**8916–8921.
17. **Liu, J. P., J. Baker, A. S. Perkins, E. J. Robertson, and A. Efstratiadis.** 1993. Mice carrying null mutations of the genes encoding insulin-like growth factor I (Igf-1) and type 1 IGF receptor (Igf1r). Cell **75:**59–72.
18. **Maksimova, N., K. Hara, A. Miyashita, I. Nikolaeva, A. Shiga, A. Nogovicina, A. Sukhomyasova, V. Argunov, A. Shvedova, T. Ikeuchi, M. Nishizawa, R. Kuwano, and O. Onodera.** 3 August 2007, posting date. Clinical, molecular and histopathological features of short stature syndrome with novel CUL7 mutation in Yakuts: new population isolate in Asia. J. Med. Genet. doi:10.1136/jmg.2007.051979.
19. **Nakamura, E., E. L. P. Abreu, Y. Awakura, T. Inoue, T. Kamoto, O. Ogawa, H. Kotani, T. Manabe, G. J. Zhang, K. Kondo, V. Nose, and W. G. Kaelin, Jr.** 2006. Clusterin is a secreted marker for a hypoxia-inducible factor-independent function of the von Hippel-Lindau tumor suppressor protein. Am. J. Pathol **168:**574–584.
20. **Nakayama, K., S. Hatakeyama, S. Maruyama, A. Kikuchi, K. Onoe, R. A. Good, and K. I. Nakayama.** 2003. Impaired degradation of inhibitory subunit of NF-kappa B (I kappa B) and beta-catenin as a result of targeted disruption of the beta-TrCP1 gene. Proc. Natl. Acad. Sci. USA **100:**8752–8757.
21. **Nakayama, K., H. Nagahama, Y. A. Minamishima, M. Matsumoto, I. Nakamichi, K. Kitagawa, M. Shirane, R. Tsunematsu, T. Tsukiyama, N. Ishida, M. Kitagawa, K. Nakayama, and S. Hatakeyama.** 2000. Targeted disruption of Skp2 results in accumulation of cyclin E and p27(Kip1), polyploidy and centrosome overduplication. EMBO J. **19:**2069–2081.
22. **Nakayama, K. I., and K. Nakayama.** 2005. Regulation of the cell cycle by SCF-type ubiquitin ligases. Semin. Cell Dev. Biol. **16:**323–333.
23. **Powell-Braxton, L., P. Hollingshead, C. Warburton, M. Dowd, S. Pitts-Meek, D. Dalton, N. Gillett, and T. A. Stewart.** 1993. IGF-I is required for normal embryonic growth in mice. Genes Dev. **7:**2609–2617.
24. **Rajkumar, K., D. Barron, M. S. Lewitt, and L. J. Murphy.** 1995. Growth retardation and hyperglycemia in insulin-like growth factor binding protein-1 transgenic mice. Endocrinology **136:**4029–4034.
25. **Skaar, J. R., T. Arai, and J. A. DeCaprio.** 2005. Dimerization of CUL7 and PARC is not required for all CUL7 functions and mouse development. Mol. Cell. Biol. **25:**5579–5589.
26. **Skaar, J. R., L. Florens, T. Tsutsumi, T. Arai, A. Tron, S. K. Swanson, M. P. Washburn, and J. A. DeCaprio.** 2007. PARC and CUL7 form atypical cullin RING ligase complexes. Cancer Res. **67:**2006–2014.
27. **Stryke, D., M. Kawamoto, C. C. Huang, S. J. Johns, L. A. King, C. A. Harper, E. C. Meng, R. E. Lee, A. Yee, L. L'Italien, P. T. Chuang, S. G. Young, W. C. Skarnes, P. C. Babbitt, and T. E. Ferrin.** 2003. BayGenomics: a resource of insertional mutations in mouse embryonic stem cells. Nucleic Acids Res. **31:**278–281.
28. **Tamemoto, H., T. Kadowaki, K. Tobe, T. Yagi, H. Sakura, T. Hayakawa, Y. Terauchi, K. Ueki, Y. Kaburagi, S. Satoh, et al.** 1994. Insulin resistance and growth retardation in mice lacking insulin receptor substrate-1. Nature **372:**182–186.
29. **Tetzlaff, M. T., W. Yu, M. Li, P. Zhang, M. Finegold, K. Mahon, J. W. Harper, R. J. Schwartz, and S. J. Elledge.** 2004. Defective cardiovascular development and elevated cyclin E and Notch proteins in mice lacking the Fbw7 F-box protein. Proc. Natl. Acad. Sci. USA **101:**3338–3345.
30. **Todaro, G. J., and H. Green.** 1963. Quantitative studies of the growth of mouse embryo cells in culture and their development into established lines. J. Cell Biol. **17:**299–313.
31. **Tsunematsu, R., K. Nakayama, Y. Oike, M. Nishiyama, N. Ishida, S. Hatakeyama, Y. Bessho, R. Kageyama, T. Suda, and K. I. Nakayama.** 2004. Mouse Fbw7/Sel-10/Cdc4 is required for notch degradation during vascular development. J. Biol. Chem. **279:**9417–9423.
32. **Tsunematsu, R., M. Nishiyama, S. Kotoshiba, T. Saiga, T. Kamura, and K. I. Nakayama.** 2006. Fbxw8 is essential for Cul1-Cul7 complex formation and for placental development. Mol. Cell. Biol. **26:**6157–6169.
33. **van der Eerden, B. C., M. Karperien, and J. M. Wit.** 2003. Systemic and local regulation of the growth plate. Endocr. Rev. **24:**782–801.
34. **Wang, Y., S. Penfold, X. Tang, N. Hattori, P. Riley, J. W. Harper, J. C. Cross, and M. Tyers.** 1999. Deletion of the Cul1 gene in mice causes arrest in early embryogenesis and accumulation of cyclin E. Curr. Biol. **9:**1191–1194.